Different promoting roles of ruthenium for the oxidation of primary and secondary alcohols on PtRu electrocatalysts

Iosif Mangoufis-Giasin,[1,2,*] Oriol Piqué,[3] Peyman Khanipour,[1,2,4] Karl J.J. Mayrhofer,[1,2] Federico Calle-Vallejo,[3,*] Ioannis Katsounaros[1,*]

1 Helmholtz-Institut Erlangen-Nürnberg for Renewable Energy (IEK-11), Egerlandstr. 3, 91058 Erlangen, Germany

2 Department of Chemical and Biological Engineering, Friedrich-Alexander-Universität Erlangen-Nürnberg (FAU), Egerlandstr. 3, 91058 Erlangen, Germany

3 Department of Materials Science and Physical Chemistry & Institute of Theoretical and Computational Chemistry (IQTCUB), University of Barcelona, Martí i Franquès 1, 08028 Barcelona, Spain

4 Bundesanstalt für Materialforschung und -prüfung (BAM), Richard-Willstätter-Str. 11, 12489 Berlin, Germany

***Corresponding authors:**

Iosif Mangoufis-Giasin (i.mangoufis@fz-juelich.de)

Dr. Federico Calle-Vallejo (f.calle.vallejo@ub.edu)

Dr. Ioannis Katsounaros (i.katsounaros@fz-juelich.de)

Abstract

This study shows remarkably different features between the oxidation of secondary and primary C_3-C_5 alcohols. The oxidation of primary alcohols is controlled by the oxidative removal of blocking adsorbates, such as CO, formed after the dissociative adsorption of alcohol molecules. Conversely, secondary alcohols do not undergo dissociative adsorption and therefore their oxidation is purely controlled by the energetics of the elementary reaction steps. In this respect, a different role of ruthenium is revealed for the electrooxidation of primary and secondary alcohols on bimetallic platinum-ruthenium catalysts. Ruthenium enhances the oxidation of primary alcohols via the established bifunctional mechanism, in which the adsorption of (hydr)oxide species that are necessary to remove the blocking adsorbates is favored. In contrast, the oxidation of secondary alcohols is enhanced by the Ru-assisted stabilization of an O-bound intermediate that is involved in the potential-limiting step. This alternative pathway enables the oxidation of secondary alcohols close to the equilibrium potential.

Keywords: electrocatalysis; electrochemical energy conversion; direct alcohol fuel cells; alcohol electrooxidation; secondary alcohols; 2-propanol oxidation; electrochemical real-time mass spectrometry; density functional theory

1. Introduction

The oxidation of primary alcohols such as methanol and ethanol has been extensively considered as an anode reaction in direct alcohol fuel cells (DAFCs), to power portable devices such as mobile phones, laptops or tablets [1,2]. The electrochemical oxidation of such alcohols has been thoroughly studied to understand reaction mechanisms and to develop efficient catalyst materials [3–5]. The state-of-the-art catalysts for the oxidation of primary alcohols are platinum-ruthenium alloys. The presence of ruthenium shifts the onset potential to lower values compared to pure platinum catalysts [6–9]. This has been explained by the ability of ruthenium to adsorb (hydr)oxide species at lower overpotential than platinum; such species act as educts for the oxidative removal of the alcohol-derived blocking adsorbates (e.g. adsorbed CO) present on platinum sites according to the bifunctional mechanism [10–14].

On the contrary, the oxidation of secondary alcohols (mainly 2-propanol), has received considerably less attention so far. This is because the C-C bond of 2-propanol is stable upon alcohol oxidation, preventing the complete conversion to CO_2 that would correspond to the maximum number of electrons exchanged per 2-propanol molecule [15–18]. This feature, however, makes 2-propanol fuel cells an attractive system, for instance when coupled with catalytic transfer hydrogenation reaction (CTHR) from liquid organic hydrogen carriers (LOHCs) [19]. Such a fuel cell oxidizes 2-propanol to acetone at the anode delivering electricity and the formed acetone is hydrogenated back to 2-propanol via CTHR using a hydrogen-rich LOHC. Finally, the 2-propanol is introduced again in the fuel cell, enabling a fully reversible cycle. This concept is thoroughly described in a recent publication [19].

The performance of a 2-propanol fuel cell in terms of OCV and power density is greatly improved if a platinum-ruthenium anode catalyst is used instead of pure platinum [19,20]. It was recently shown that this is due to the ability of PtRu/C to activate 2-propanol at low overpotential, close to the equilibrium potential of the 2-propanol/acetone couple [21]. Even though ruthenium enhances the oxidation of either primary alcohols or 2-propanol, there are two clear indications that the effect of ruthenium for the oxidation of 2-propanol is different than for primary alcohols: First, the absence of adsorbed CO and the stability of the C-C bond when 2-propanol is oxidized [22] imply

that ruthenium does not enhance this reaction via the removal of surface-adsorbed carbon-containing species, as these are anyway not present at the surface. Second, the beneficial effect of ruthenium is not manifested as a negative shift of the onset potential of 2-propanol oxidation, as it does for primary alcohols, but as a new oxidation process at lower potentials clearly separated from the one on pure platinum [21]. We note that the ideal anode catalyst for integration into an LOHC/2-propanol system should not enable C-C bond splitting, which is a remarkable difference compared to classical anodes for DAFC applications based on primary alcohols.

Here, we aim to understand the origin of the beneficial effect of ruthenium for the oxidation of 2-propanol and investigate whether this effect is a general characteristic of secondary alcohols. To this end, we compare the oxidation of primary and secondary alcohols with three, four and five carbon atoms, on Pt/C and PtRu/C, using rotating disc electrode (RDE) and electrochemical real-time mass spectrometry (EC-RTMS) measurements. Besides, the experiments are supplemented by density functional theory (DFT) calculations. Our results highlight a remarkably different effect of ruthenium for the oxidation of primary and secondary alcohols: while primary alcohol oxidation is favored via the ruthenium-assisted adsorption of oxygenates which removes blocking adsorbates, the oxidation of secondary alcohols is favored because ruthenium stabilizes a different intermediate compared to Pt/C, thereby opening another reaction pathway that is feasible at lower potential.

2. Materials and methods

2.1 Electrocatalyst preparation

Both electrocatalysts used in this study (Pt/C and PtRu/C) were commercial nanoparticles from Tanaka; details on the catalyst characteristics, as provided by the manufacturer, are summarized in our previous work [21]. The nanoparticles were dispersed using an SFX150 Horn Sonifier (Branson, USA), in ultrapure water in the case of PtRu/C and in ultrapure water with addition of 2-propanol (water:2-propanol volume ratio 3:1) in the case of Pt/C. The resulting homogeneous catalyst ink was pipetted onto a glassy carbon disk (embedded on Teflon shroud, PINE) for RDE measurements or on a glassy carbon (GC) plate (HTW Hochtemperatur-Werkstoffe GmbH) for EC-RTMS measurements. The drop-casted suspension was left to dry in the air, resulting in a thin catalyst film on the GC substrate, which acted as the working electrode; the final Pt loading was 25 $\mu g_{Pt}\,cm^{-2}$. Both GC substrates (disks or plates) were polished before each deposition with diamond paste (0.25 μm, Saint-Gobain Diamantwerkzeug GmbH).

2.2 Electrochemical measurements

Unless complementary product analysis was performed, the electrochemical measurements were conducted in a RDE setup, using a custom-made Teflon cell and a PINE MSR Electrode Rotator. When products were analyzed in real time, the electrochemical measurements were performed using a V-type flow cell coupled to EC-RTMS (as described in section 2.3) [23]. The counter electrode was a platinum wire (Mateck GmbH) and the reference electrode was a Ag/AgCl in 3.0 mol L^{-1} KCl (Metrohm). All potentials in the manuscript are expressed with respect to the reversible hydrogen electrode (RHE), determined by measuring the open circuit potential of a platinum wire versus the Ag/AgCl in a hydrogen-saturated 0.1 mol L^{-1} $HClO_4$ solution. For RDE measurements, the reference electrode was kept in a separate compartment connected to the main compartment by a Luggin capillary to avoid contamination from chloride ions. For EC-RTMS measurements, the platinum counter electrode was placed at the waste channel, separated from the collection capillary (see below), to avoid any interference with product analysis. The electrolyte was sparged with Argon (Air Liquide, 4.8N) prior to each measurement for 20 min to deaerate the electrolyte, and the gas flow was then maintained throughout the entire experiment. To form a CO monolayer, the electrolyte was saturated with carbon monoxide (Air Liquide, 4.7N) for 10 min, while the working electrode was at +0.075 V *vs* RHE. Afterwards, the electrolyte was sparged with Ar for 40 min by keeping the electrode at the same potential, to ensure that there was no CO left in the solution. The procedure to form a partial CO layer is described in the supporting information, section S1, together with the respective data. The electrolyte was prepared by dissolving concentrated $HClO_4$ (70%, Merck Suprapure) and the appropriate alcohol (Merck Suprapure) in ultrapure water (Merck Millipore, resistance 18.2 MΩ·cm, TOC < 3 ppb). A Gamry Reference600 potentiostat was used to perform the electrochemical measurements. The electrolyte resistance was determined before each measurement with electrochemical impedance spectroscopy and compensation (by 90%) was performed using positive feedback; the remaining uncompensated resistance was always below 4 Ω, independent of the used cell configuration.

2.3 Electrochemical real-time mass spectrometry

The EC-RTMS principles for the characterization of liquid and gaseous reaction products shortly after their formation have been described in previous works [23,24]. In brief, a collection capillary is positioned close (ca. 100 μm) to the working electrode surface. The electrolyte together with reaction products is continuously withdrawn for analysis with a combination of two mass

spectrometry techniques. In this manuscript, the dissolved ketone (acetone, butanone, 2-pentanone or 3-pentanone) which was formed after the oxidation of the respective secondary alcohol (2-propanol, 2-butanol, 2-pentanol or 3-pentanol, respectively) was analyzed using a direct analysis in real time - time of flight mass spectrometer (DART-TOF-MS, JEOL JMS-T100LP AccuTOF). The mass ranges used for the characterization were: m/z = 60.0−60.1 for acetone (ion structure $[^{13}C^{12}C_2H_6O + H]^+$), m/z = 74.0−74.1 for 2-butanone (ion structure $[^{13}C^{12}C_3H_8O + H]^+$) and m/z = 88.0−88.2 for 2- or 3-pentanone (ion structure $[^{13}C^{12}C_4H_{10}O + H]^+$). Carbon dioxide, extracted from the electrolyte via a homemade degasser [23], was analyzed with an electron impact-quadrupole mass spectrometer (EI-QMS, Extrel MAX300-LG) at m/z = 44.

2.4 Computational details

The VASP code [25] was used to carry out the DFT simulations with the Perdew-Burke-Ernzerhof (PBE) exchange-correlation functional and the PAW method [26,27]. To model Pt and PtRu, two different surface models were used: Pt(111) terraces, and $Pt_{0.5}Ru_{0.5}$(111) terraces (denoted PtRu(111)). We used (2×2) supercell slabs containing 4 atomic layers to build the slab models. Converged PBE lattice constants of 3.98 Å and 3.90 Å were employed to build the Pt(111) and PtRu(111) models, respectively. The adsorbates and the top two layers of the slabs were allowed to relax in all directions, while the bottom layers were fixed at the bulk equilibrium distances. A plane-wave cutoff of 450 eV was used in all the calculations. The smearing of the Fermi level was performed with the Methfessel-Paxton approach, using an electronic temperature of 0.2 eV, and the total energies were extrapolated to 0 K. The numerical integration in the reciprocal space was carried out using Monkhorst-Pack grids of 6×6×1 for both slab models, which guaranteed convergence of the adsorption energies within ±0.05 eV. The repeated images were separated by more than 13 Å of vacuum in the vertical direction and dipole corrections were also applied. The conjugate-gradient optimization algorithm was used for the geometry optimizations, with iterations performed until the maximal force on all atoms was below 0.05 $eV \cdot Å^{-1}$. Asymmetric boxes of 9×10×11 $Å^3$ were used to calculate the isolated molecules in this study, considering the Γ-point only and an electronic temperature of 0.001 eV.

The reaction free energies were approximated as $\Delta G \approx \Delta E_{DFT} + \Delta ZPE - T\Delta S + \Delta E_{solvation}$, where ΔE_{DFT} is the DFT-calculated reaction energy, ΔZPE is the zero-point energy change, $T\Delta S$ is the corresponding entropy change at 298.15 K, and $\Delta E_{solvation}$ contains ad-hoc solvation corrections depending on the chemical nature of the adsorbates [28] (see further details and specific values in section S7 of the SI). The ΔS values of free molecules were obtained from thermodynamic tables, while for adsorbates ΔS only includes vibrational entropies. Vibrational frequency analyses were

used to obtain the values of *ZPE* and S_{vib}, making use of the harmonic oscillator approximation. Gas-phase corrections were applied to ensure that the calculated equilibrium potentials match the experimental ones [29] (see further details and specific values in the section S6 of the SI). The computational hydrogen electrode was used to model proton-electron pairs [30]. We did not compute proton-electron transfer barriers in this study, as Rossmeisl et al. recently noted that there is "not (yet) a method to obtain electrochemical barriers between realistic states at constant electrochemical conditions" [31]. The adsorption energies of all the intermediates featured in this study can be found in section S8 of the SI. Moreover, the most stable optimized geometries for each intermediate can be found in section S9 of the SI.

3. Results and discussion

The electrooxidation of primary and secondary C_3-C_5 alcohols on Pt/C is depicted in the positive-going linear sweep voltammograms (LSVs) in **Fig. 1** (the full cycles are shown in Section 2 of the SI). We only used the positive direction of the scan to draw conclusions because the reverse scan is strongly affected by the upper vertex potential and the associated formation of platinum oxide. The oxidation current for each secondary alcohol (red curves) is always significantly higher than that for the primary alcohol of equal chain length (blue curves). For example, the peak current density for 2-propanol oxidation (ca. 80 mA cm^{-2}) is more than ten times higher than for 1-propanol (ca. 6.5 mA cm^{-2}). When one molecule of 2-propanol is oxidized on platinum (selectively to acetone [21]) only two electrons are transferred, while the 1-propanol oxidation forms a variety of products that require the transfer of equal or higher number of electrons ($2e^-$ for propanal, $4e^-$ for propionic acid and $18e^-$ for carbon dioxide formation [24]). Therefore, considering that more electrons are exchanged on average per alcohol molecule when 1-propanol is oxidized, the higher currents for the oxidation of secondary alcohols point toward more facile kinetics compared to the oxidation of primary alcohols. This conclusion is in line with the lower onset potentials for the secondary compared to the primary alcohols; for example, 2-propanol oxidation starts at ca. +0.3 V *vs* RHE, i.e. 300 mV more negative than the oxidation of 1-propanol. Moreover, when comparing the currents within each alcohol type, the maximum current density decreases along the series 1-PrOH > 1-BuOH > 1-PeOH, and 2-PrOH > 2-BuOH > 2-PeOH ≈ 3-PeOH (see Figure S3 in the SI). A summary of the onset potentials and peak current densities for all alcohols on Pt/C can be found in Table S1 of the SI. In the reverse scan, the reduction of the platinum oxide which was formed at high potentials and suppressed the reaction, renders platinum sites available again to oxidize the respective alcohol, giving rise to the oxidation current (see Figure S2 in the SI).

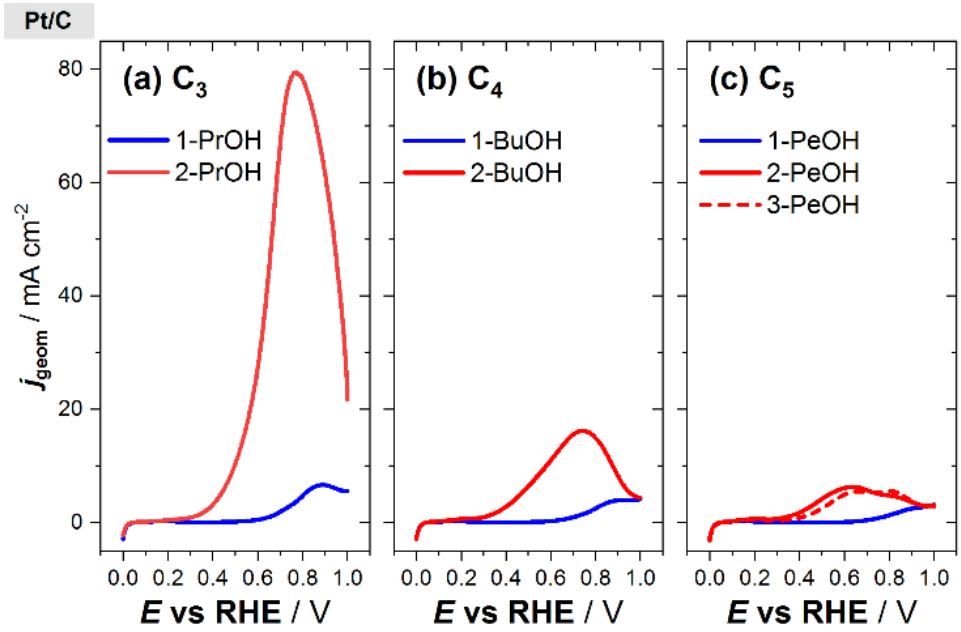

Figure 1. Electrooxidation of studied alcohols on Pt/C: Positive-going LSVs in 0.1 mol L^{-1} $HClO_4$ in the presence of 0.2 mol L^{-1} of the primary or secondary alcohol indicated in the legend: (a) C_3H_7OH, (b) C_4H_9OH, (c) $C_5H_{11}OH$. Scan rate: 5 mV s^{-1}. Rotation rate: 1600 rpm. Full cycles are shown in Section 2 of the SI.

Similarly to Pt/C, secondary alcohols are more active toward oxidation compared to the respective primary alcohol on PtRu/C (**Fig.2**), and the oxidation currents decrease by increasing the chain length, for both primary and secondary alcohols (SI, Figure S3). In the presence of ruthenium, however, a new oxidation peak emerges for all four secondary alcohols at ca. +0.15 V *vs* RHE, with an onset at ca. +0.05 V *vs* RHE. The ability of PtRu/C to activate 2-propanol at such low potential, close to the equilibrium potential [21], is responsible for the high OCV (ca. 0.8 V) measured in 2-propanol fuel cells when a PtRu/C anode is used [19]. We recently proposed that the oxidation of 2-propanol in this potential region takes place on active sites consisting of Pt-Ru ensembles, based on the observation that platinum-free ruthenium is inactive. This was also supported by the fact that continuous potential cycling led to gradual ruthenium dissolution and the disappearance of the oxidation peak at low potential [21]. At higher potential the availability of the Pt-Ru ensembles decreases due to ruthenium oxidation, leading to a suppression of the oxidation current until the potential is positive enough to activate 2-propanol on sites that consist exclusively of platinum [21]. **Fig. 2** shows that the above description can be expanded to all secondary alcohols studied here, as long as both platinum and ruthenium are present at the surface. Similar to Pt/C, platinum oxide is reduced in the negative-going scan leading to the oxidation of the respective alcohol again. However, the characteristic oxidation peak at low overpotential is absent in all of the secondary alcohols studied (Fig. S3 of the SI). This further supports the notion that the ruthenium oxidation is detrimental for the oxidation reaction in the low overpotential region. Note that the rotation rate of the electrode has an impact on the current density during the LSV on PtRu/C (see Figure S6 in the SI), suggesting that the oxidation current

involves, at least in part, 2-propanol molecules which are transported from the electrolyte to the electrode.

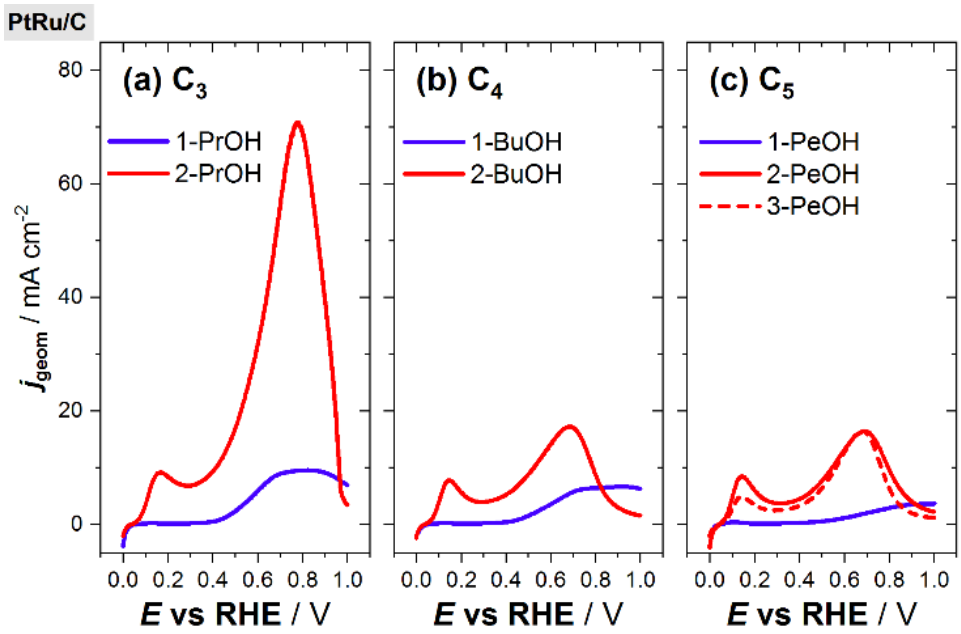

Figure 2. Electrooxidation of studied alcohols on PtRu/C: Positive-going LSVs in 0.1 mol L^{-1} $HClO_4$ in the presence of 0.2 mol L^{-1} of the primary or secondary alcohol indicated in the legend: (a) C_3H_7OH, (b) C_4H_9OH, (c) $C_5H_{11}OH$. Scan rate: 5 mV s^{-1}. Rotation rate: 1600 rpm. Full cycles are shown in Section 2 of the SI.

To verify whether the oxidation of each alcohol yields the respective ketone in the entire potential range, we analyzed the products of the oxidation of all C_3-C_5 alcohols investigated here on PtRu/C. **Fig. 3** shows the mass signals for the respective ketone (bottom panels) and CO_2 (top panels) for the oxidation of each alcohol, as indicated on top of the figures. The products were monitored parallel to a LSV in the positive direction. Note that the reactant concentration was adjusted for each alcohol to avoid interferences with product analysis and that the ionization efficiency is matrix-dependent so it varies strongly on the nature of the used alcohol. Therefore, the recorded mass intensities (Y-axis) in **Fig. 3** can be assessed only qualitatively and labels are intentionally not shown, to avoid misleading the reader. Indeed, the mass signal profiles for the detected ketones match well with the corresponding current density profiles from **Fig. 2**, including the early oxidation peak at +0.15 V *vs* RHE, whereas in all cases only traces of CO_2 were detected, only above ca. +0.6 V *vs* RHE. The careful inspection of the full mass spectrum from the time-of-flight mass analyzer did not reveal any changes in signals which would be associated with the formation of other reaction products. In addition, the use of a non-porous membrane for the gas-liquid separation (Teflon™ AF-2400) suppresses the permeation of volatiles which could get ionized and fragmented during the electron ionization, as shown previously [24], hence we can safely assign the m/z = 44 to CO_2.

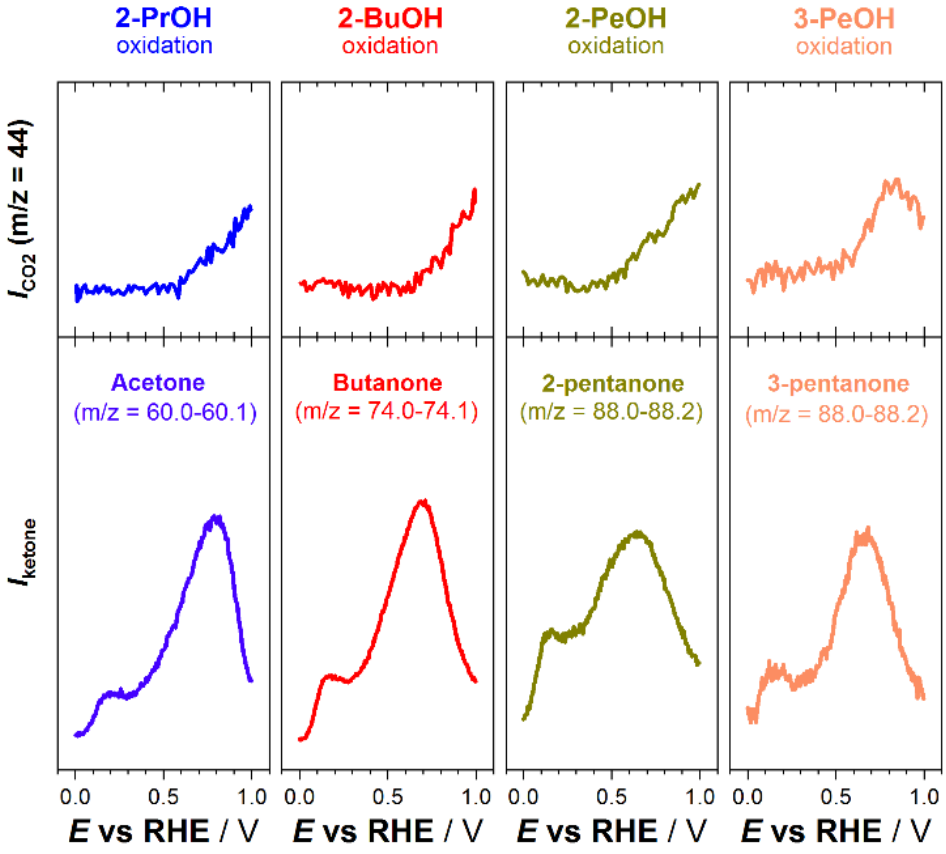

Figure 3. Product analysis during the electrooxidation of alcohols on PtRu/C, using a flow cell coupled to EC-RTMS. Positive-going linear scans in 0.1 mol L^{-1} $HClO_4$ in the presence of the secondary alcohol indicated on top of the figure. The top panel shows the mass signal for the respective ketone as indicated in the legend, detected with the DART-TOF-MS, whereas the top panels show always the mass signal at the EI-QMS for m/z = 44, which is assigned to CO_2.

To reach a molecular-level understanding on the role of surface ruthenium atoms in the activation of the secondary alcohols at such low overpotential, we used DFT calculations to investigate the oxidation of 1-propanol to propanal and the oxidation of 2-propanol to acetone. **Fig. 4** shows the most favourable pathways for these conversions on Pt(111) and PtRu(111). We chose to study the simpler, shorter-chain alcohols as the model molecules for all other primary and secondary alcohols, since they represent the most computationally affordable models and the growth of the hydrocarbon chain will probably not lead to different conclusions. For the oxidation of 1-propanol to propanal (**Fig. 4a**), the first dehydrogenation step is potential-limiting on both surfaces, but the onset potential is significantly lower for PtRu(111) by ~0.27 V (0.58 V for Pt(111) versus 0.31 V for PtRu(111)). Interestingly, the adsorbed intermediates resulting from the first dehydrogenation are different on the two surfaces. On Pt(111), adsorption at top sites and dehydrogenation occurs via the alpha carbon (Cα) of 1-propanol (*CH_3CH_2CHOH), while on PtRu(111) the O atom of the

hydroxyl group is dehydrogenated (*CH_3CH_2CHO) and binds to the surface on bridge sites. It is likely that the dehydrogenation of the O-bound intermediate goes through the simultaneous making of a C-surface bond and the breaking of a C-H bond, leading to adsorbed propionaldehyde.

Similarly, the free-energy diagram for the most favorable pathway for the oxidation of 2-propanol to acetone (**Fig. 4b**), shows that the first dehydrogenation step determines the onset potential on both surfaces and the onset potential on PtRu(111) is lower than on Pt(111). Moreover, 2-propanol oxidizes to acetone via an O-bound intermediate (*$(CH_3)_2CHO$), whereas the first intermediate on Pt(111) (*$(CH_3)_2COH$) adsorbs through the Cα atom. The intermediates bind to the surface similarly to those corresponding to 1-propanol oxidation. Note in passing that the DFT-calculated onset potentials are not to be compared directly with the experimental ones, as they were calculated for (111) surface terminations as a first approximation.

We note that previous heterogeneous catalysis studies showed that the different reactivity of 1-propanol and 2-propanol is correlated with the higher stability of the C-C bonds in 2-propanol, owing to the electron donor character of the two methyl groups in the latter [32]. Besides, other studies showed that H_2O molecules promote the liquid-phase oxidation of alcohols on Pt, in line with our findings, as water-adsorbate interactions help in stabilizing the reaction intermediates. This is desirable to lower the overpotential, as all of the intermediates and products are above the energy level of the reactants at 0 V vs RHE (see Figure 4) [33].

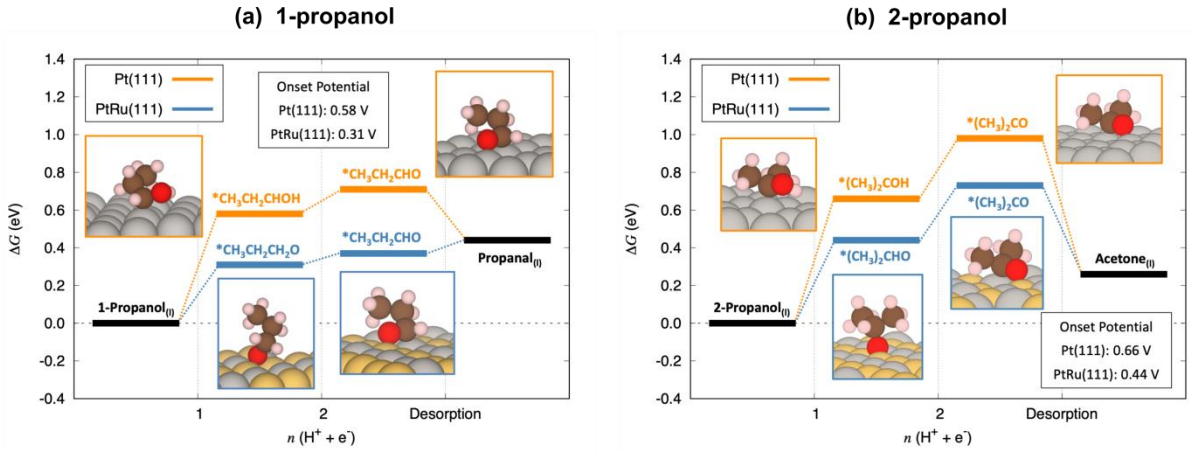

Figure 4. Free-energy diagram of the most favorable pathway at 0 V *vs* RHE for (a) 1-propanol oxidation to propanal, and (b) 2-propanol oxidation to acetone. In orange, Pt(111); in blue, PtRu(111). The calculated onset potentials and optimized geometries of the intermediates are also included. Pt, Ru, O, C and H atoms are shown in grey, yellow, red, brown and pink.

In brief, the DFT calculations indicate that on an adsorbate-free surface, the oxidation of either 1- or 2-propanol in presence of ruthenium would open a new pathway compared to Pt(111), where the first intermediate is an O-bound adsorbate. However, it is known that primary alcohols undergo dissociative adsorption on platinum, forming C-(CO) adsorbates, contrary to secondary alcohols [13–16,31]. The dissociative adsorption of primary alcohols is evidenced by (i) the detection of adsorbed CO below the oxide region, (ii) the oxidative stripping of adsorbates to gaseous CO_2 at the onset of oxide formation, and (iii) the reductive formation of C_{n-1} hydrocarbons when the potential of the platinum electrode is in the hydrogen under-potential deposition region and in contact with a solution containing a C_n primary alcohol [13,14]. All these features are absent for secondary alcohols.

Fig. 5 shows the positive-going LSVs for the oxidation of 1-propanol (solid blue) and 2-propanol (dashed blue), on Pt/C and PtRu/C. Moreover, the curve for the oxidative stripping of a pre-adsorbed CO sub-monolayer (see section S1 in the SI for details) in a 0.1 M $HClO_4$ solution free from CO or any alcohol is superimposed (in red). The comparison of the voltammograms in **Fig. 5a** and **Fig. 5b** shows that independent of the catalyst, the onset of 1-propanol oxidation is similar to the onset of CO oxidation, while the oxidation of 2-propanol commences at significantly lower potentials by ca. 400 mV. Note that we used carbon monoxide only as a model blocking adsorbate, being aware that the nature and the coverage of the surface adsorbates that are formed after the dissociative adsorption of 1-propanol on Pt/C or PtRu/C are likely different.

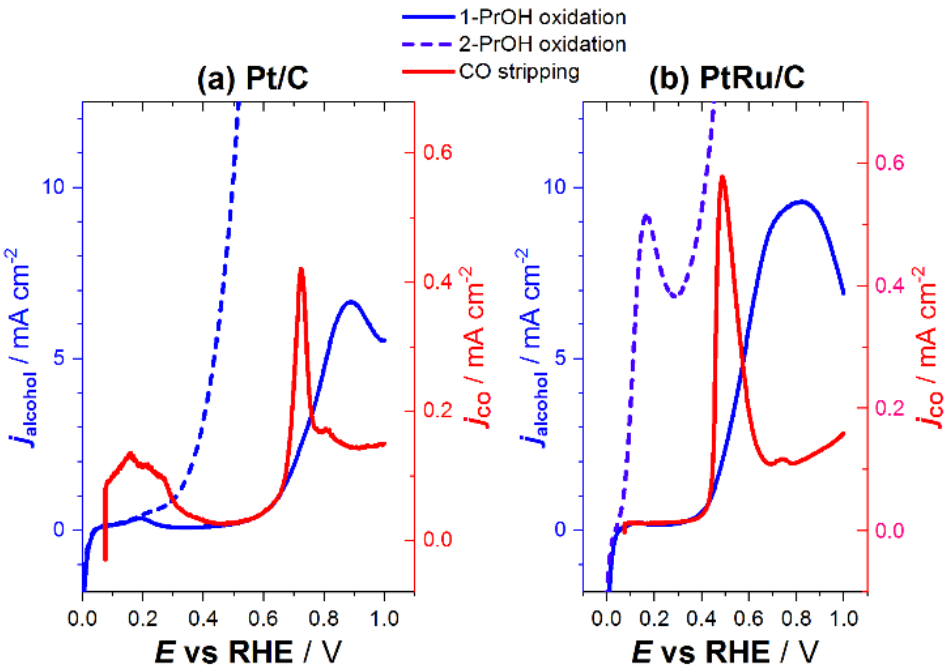

Figure 5. Linear sweep voltammograms (positive direction), in 0.1 M $HClO_4$ for CO stripping and 0.1 mol L^{-1} $HClO_4$ + 0.2 mol L^{-1} 1-propanol or 2-propanol with a scan rate of 5 mV s^{-1} on (a) Pt/C or (b) PtRu/C.

For Pt/C, the layer was formed after the partial oxidation of a complete CO adlayer, as described in the SI, section S1.

The good match between the onsets for the oxidation of 1-propanol and CO for both catalyst, indicates that the oxidation of 1-propanol is controlled by the oxidative removal of adsorbates formed after dissociative *C-CO adsorption [15], which block the active sites. In that case, the role of ruthenium on the oxidation of 1-propanol is merely to shift the onset potential of the adsorption of (hydr)oxide species, which in turn lowers the potential for the oxidative removal of the blocking adsorbates, thereby lowering the onset of 1-propanol oxidation, as described by the well-established bifunctional mechanism for the oxidation of methanol and ethanol [10,12,34,35]. Therefore, the sites necessary for the stabilization of the O-bound intermediate and the change in the reaction pathway, as predicted by DFT for the clean PtRu(111) surface, are not accessible under experimental conditions, because of the surface blocking with carbonaceous adsorbates.

On the contrary, the oxidation of 2-propanol is not controlled by the coverage of adsorbed CO or other chemisorbed species, as the alcohol does not adsorb dissociatively. Moreover, the acetone molecules that formed and did not desorb [22], remain molecularly intact and do not dissociate except for Pt(100) terraces, as demonstrated in a recent article on the adsorption of acetone on platinum single-crystalline surfaces [36]. The absence of blocking carbon-based adsorbates results in a lower onset potential for 2-propanol compared to 1-propanol on Pt/C, in a potential region where blocking species such as CO are stable and would inhibit the reaction if they were present, as they do for 1-propanol (see **Fig. 5a**). Additionally, on PtRu/C, the absence of products of dissociative adsorption renders the Pt-Ru ensemble sites available to adsorb the first intermediate of the dehydrogenation reaction via the O atom, as indicated by DFT. Therefore, we propose that the new oxidation process at low overpotential in the presence of ruthenium, which is a striking feature observed experimentally only for secondary alcohols, originates from the alteration of the reaction pathway due to the stabilization of a different intermediate compared to Pt(111). Presumably, this process would likely be possible also for 1-propanol oxidation (as described by **Fig. 4a**) if the latter did not dissociate upon adsorption. These conclusions can be extended to the longer carbon-chain molecules, considering that the onset potentials are practically identical within the same alcohol type (primary or secondary) (see Table S1 in the SI).

The above discussion has implications for two additional observations from **Fig. 1** and **Fig. 2**. First, the decreasing electrocatalytic activity as the carbon chain length increases for either primary or secondary alcohols can be attributed to steric hindrance. For primary alcohols, the dissociative adsorption of longer-chain alcohol leads to decreased surface availability from

adsorbates that contain more carbon atoms. For secondary alcohols, the steric hindrance likely originates from the formed ketone which remains adsorbed as shown previously for acetone during 2-propanol oxidation [22]. Similarly, the significantly lower currents for the oxidation of primary alcohols compared to their isomers can be explained by the stronger inhibition caused by adsorbed blocking species.

4. Conclusions

We studied the oxidation of primary and secondary alcohols with three, four and five carbon atoms on platinum and platinum-ruthenium catalysts. The secondary alcohols 2-propanol, 2-butanol, 2-pentanol and 3-pentanol are oxidized on either Pt/C or PtRu/C to the respective ketone. On Pt/C, the onset potential of their oxidation is more negative than for the respective primary alcohols 1-propanol, 1-butanol and 1-pentanol. On PtRu/C, a new oxidation process emerges at low overpotential, only for secondary alcohols. DFT calculations show the same trends for the dehydrogenation of 1-propanol and 2-propanol. In particular, a C-bound intermediate determines the onset potential on Pt(111), whereas on PtRu(111), ruthenium stabilizes a different, O-bound intermediate for both alcohols, lowering the onset potential. However, under experimental conditions, the dissociative adsorption of primary alcohols blocks the sites that can adsorb the critical O-bound intermediate, so the pathway predicted from DFT is inaccessible and the oxidation of primary alcohols is controlled by the (hydr)oxide-promoted desorption of these inhibiting species. On the contrary, this limitation is not present during the oxidation of secondary alcohols which do not undergo dissociative adsorption, so the adsorption of the O-bound intermediate is possible and the reaction is controlled by the adsorption/dehydrogenation step of the alcohol.

Therefore, while ruthenium is known to promote alcohol oxidation via the earlier adsorption of (hydr)oxide species, this conclusion must be limited to primary alcohols only. This work reveals a different role of ruthenium in the oxidation of secondary alcohols, which is independent of the adsorption of (hydr)oxide species and is directly related to the alcohol dehydrogenation intermediates.

Acknowledgements

This work was funded by the Bavarian Ministry of Economic Affairs, Regional Development and Energy. F.C.-V. acknowledges funding from Spanish MICIUN RTI2018-095460-B-I00, Ramón y

Cajal RyC-2015-18996 and María de Maeztu MDM-2017-0767 grants and partly by Generalitat de Catalunya 2017SGR13. O.P. thanks the Spanish MICIUN for a PhD grant (PRE2018-083811). We thank Red Española de Supercomputación (RES) for supercomputing time at SCAYLE (projects QS-2019-3-0018, QS-2019-2-0023, and QCM-2019-1-0034), MareNostrum (project QS-2020-1-0012), and CENITS (project QS-2020-2-0021). The use of supercomputing facilities at SURFsara was sponsored by NWO Physical Sciences, with financial support by NWO.

References

[1] A.S. Aricò, S. Srinivasan, V. Antonucci, DMFCs: From Fundamental Aspects to Technology Development, Fuel Cells. 1 (2001) 133–161. https://doi.org/10.1002/1615-6854(200107)1:2<133::aid-fuce133>3.3.co;2-x.

[2] C. Lamy, A. Lima, V. LeRhun, F. Delime, C. Coutanceau, J.M. Léger, Recent advances in the development of direct alcohol fuel cells (DAFC), J. Power Sources. 105 (2002) 283–296. https://doi.org/10.1016/S0378-7753(01)00954-5.

[3] C. Lamy, E.M. Belgsir, J.M. Léger, Electrocatalytic oxidation of aliphatic alcohols: Application to the direct alcohol fuel cell (DAFC), J. Appl. Electrochem. 31 (2001) 799–809. https://doi.org/10.1023/A:1017587310150.

[4] T. Iwasita-Vielstich, Progress in the study of methanol oxidation by in situ, ex situ and on-line methods, Adv. Electrochem. Sci. Eng. 1 (2008) 127–170. https://doi.org/10.1002/9783527616756.ch3.

[5] E. Peled, T. Duvdevani, A. Aharon, A. Melman, New fuels as alternatives to methanol for direct oxidation fuel cells, Electrochem. Solid-State Lett. 4 (2001). https://doi.org/10.1149/1.1355036.

[6] M.M.P. Janssen, J. Moolhuysen, Binary systems of platinum and a second metal as oxidation catalysts for methanol fuel cells, Electrochim. Acta. 21 (1976) 869–878. https://doi.org/10.1016/0013-4686(76)85059-1.

[7] B. Beden, F. Kadirgan, C. Lamy, J.M. Leger, Electrocatalytic oxidation of methanol on platinum-based binary electrodes, J. Electroanal. Chem. 127 (1981) 75–85. https://doi.org/10.1016/S0022-0728(81)80469-X.

[8] M. Watanabe, M. Uchida, S. Motoo, Preparation of highly dispersed Pt + Ru alloy clusters and the activity for the electrooxidation of methanol, J. Electroanal. Chem. 229 (1987) 395–406. https://doi.org/10.1016/0022-0728(87)85156-2.

[9] J.B. Goodenough, A. Hamnett, B.J. Kennedy, R. Manoharan, S.A. Weeks, Methanol oxidation on unsupported and carbon supported Pt + Ru anodes, J. Electroanal. Chem. 240 (1988) 133–145. https://doi.org/10.1016/0022-0728(88)80318-8.

[10] H.A. Gasteiger, N. Markovic, P.N. Ross, E.J. Cairns, Methanol Electrooxidation on Well-Characterized Pt-Ru Alloys, 97 (1993) 12020–12029.

[11] H.A. Gasteiger, N. Markovic, P.N. Ross, E.J. Cairns, CO electrooxidation on well-characterized Pt-Ru alloys, J. Phys. Chem. 98 (1994) 617–625. https://doi.org/10.1021/j100053a042.

[12] N.M. Marković, H.A. Gasteiger, P.N. Ross, X. Jiang, I. Villegas, M.J. Weaver, Electro-

oxidation mechanisms of methanol and formic acid on Pt-Ru alloy surfaces, Electrochim. Acta. 40 (1995) 91–98. https://doi.org/10.1016/0013-4686(94)00241-R.

[13] J. Schnaidt, Z. Jusys, R.J. Behm, Electrooxidation of 1-propanol on Pt - Mechanistic insights from a spectro-electrochemical study using isotope labeling, J. Phys. Chem. C. 116 (2012) 25852–25867. https://doi.org/10.1021/jp3086733.

[14] E. Pastor, S. Wasmus, T. Iwasita, M.C. Arévalo, S. González, A.J. Arvia, Spectroscopic investigations of C3 primary alcohols on platinum electrodes in acid solutions. Part I. n-propanol, J. Electroanal. Chem. 350 (1993) 97–116. https://doi.org/10.1016/0022-0728(93)80199-R.

[15] J.F.E. Gootzen, A.H. Wonders, W. Visscher, J.A.R. Van Veen, Adsorption of C3 alcohols, 1-butanol, and ethene on platinized platinum as studied with FTIRS and DEMS, Langmuir. 13 (1997) 1659–1667. https://doi.org/10.1021/la960991n.

[16] I.D.A. Rodrigues, J.P.I. De Souza, E. Pastor, F.C. Nart, Cleavage of the C-C bond during the electrooxidation of 1-propanol and 2-propanol: Effect of the Pt morphology and of codeposited Ru, Langmuir. 13 (1997) 6829–6835. https://doi.org/10.1021/la9704415.

[17] J.F. Gomes, V.L. Oliveira, P.M.P. Pratta, G. Tremiliosi-Filho, Reactivity of Alcohols with Three-Carbon Atom Chain on Pt in Acidic Medium, Electrocatalysis. 6 (2015) 7–19. https://doi.org/10.1007/s12678-014-0218-x.

[18] E. Pastor, S. González, A.J. Arvia, Electroreactivity of isopropanol on platinum in acids studied by DEMS and FTIRS, J. Electroanal. Chem. 395 (1995) 233–242. https://doi.org/10.1016/0022-0728(95)04129-C.

[19] G. Sievi, D. Geburtig, T. Skeledzic, A. Bösmann, P. Preuster, O. Brummel, F. Waidhas, M.A. Montero, P. Khanipour, I. Katsounaros, J. Libuda, K.J.J. Mayrhofer, P. Wasserscheid, Towards an efficient liquid organic hydrogen carrier fuel cell concept, Energy Environ. Sci. 12 (2019) 2305–2314. https://doi.org/10.1039/c9ee01324e.

[20] D. Cao, S.H. Bergens, A direct 2-propanol polymer electrolyte fuel cell, J. Power Sources. 124 (2003) 12–17. https://doi.org/10.1016/S0378-7753(03)00613-X.

[21] P. Khanipour, F.D. Speck, I. Mangoufis-Giasin, K.J.J. Mayrhofer, S. Cherevko, I. Katsounaros, Electrochemical Oxidation of Isopropanol on Platinum-Ruthenium Nanoparticles Studied with Real-Time Product and Dissolution Analytics, ACS Appl. Mater. Interfaces. 12 (2020) 33670–33678. https://doi.org/10.1021/acsami.0c07190.

[22] F. Waidhas, S. Haschke, P. Khanipour, L. Fromm, A. Görling, J. Bachmann, I. Katsounaros, K.J.J. Mayrhofer, O. Brummel, J. Libuda, Secondary Alcohols as Rechargeable Electrofuels: Electrooxidation of Isopropyl Alcohol at Pt Electrodes, ACS Catal. 10 (2020) 6831–6842. https://doi.org/10.1021/acscatal.0c00818.

[23] P. Khanipour, M. Löffler, A.M. Reichert, F.T. Haase, K.J.J. Mayrhofer, I. Katsounaros, Electrochemical Real-Time Mass Spectrometry (EC-RTMS): Monitoring Electrochemical Reaction Products in Real Time, Angew. Chemie - Int. Ed. 58 (2019) 7273–7277. https://doi.org/10.1002/anie.201901923.

[24] P. Khanipour, S. Haschke, J. Bachmann, K.J.J. Mayrhofer, I. Katsounaros, Electrooxidation of saturated C1-C3 primary alcohols on platinum: Potential-resolved product analysis with electrochemical real-time mass spectrometry (EC-RTMS), Electrochim. Acta. 315 (2019) 67–74. https://doi.org/10.1016/j.electacta.2019.05.070.

[25] R.A. Vargas-Hernández, Bayesian Optimization for Calibrating and Selecting Hybrid-Density Functional Models, J. Phys. Chem. A. 124 (2020) 4053–4061. https://doi.org/10.1021/acs.jpca.0c01375.

[26] J.P. Perdew, K. Burke, M. Ernzerhof, Generalized gradient approximation made simple, Phys. Rev. Lett. 77 (1996) 3865–3868. https://doi.org/10.1103/PhysRevLett.77.3865.

[27] D. Joubert, From ultrasoft pseudopotentials to the projector augmented-wave method, Phys. Rev. B - Condens. Matter Mater. Phys. 59 (1999) 1758–1775. https://doi.org/10.1103/PhysRevB.59.1758.

[28] C.J. Bondue, F. Calle-Vallejo, M.C. Figueiredo, M.T.M. Koper, Structural principles to steer the selectivity of the electrocatalytic reduction of aliphatic ketones on platinum, Nat. Catal. 2 (2019) 243–250. https://doi.org/10.1038/s41929-019-0229-3.

[29] L.P. Granda-Marulanda, A. Rendón-Calle, S. Builes, F. Illas, M.T.M. Koper, F. Calle-Vallejo, A Semiempirical Method to Detect and Correct DFT-Based Gas-Phase Errors and Its Application in Electrocatalysis, ACS Catal. 10 (2020) 6900–6907. https://doi.org/10.1021/acscatal.0c01075.

[30] J.K. Nørskov, J. Rossmeisl, A. Logadottir, L. Lindqvist, J.R. Kitchin, T. Bligaard, H. Jónsson, Origin of the overpotential for oxygen reduction at a fuel-cell cathode, J. Phys. Chem. B. 108 (2004) 17886–17892. https://doi.org/10.1021/jp047349j.

[31] A. Bagger, L. Arnarson, M.H. Hansen, E. Spohr, J. Rossmeisl, Electrochemical CO Reduction: A Property of the Electrochemical Interface, J. Am. Chem. Soc. 141 (2019) 1506–1514. https://doi.org/10.1021/jacs.8b08839.

[32] P.C.D. Mendes, R. Costa-Amaral, J.F. Gomes, J.L.F. Da Silva, The influence of hydroxy groups on the adsorption of three-carbon alcohols on Ni(111), Pd(111) and Pt(111) surfaces: A density functional theory study within the D3 dispersion correction, Phys. Chem. Chem. Phys. 21 (2019) 8434–8444. https://doi.org/10.1039/c9cp00752k.

[33] F. Liu, H. Wang, A. Sapi, H. Tatsumi, D. Zherebetskyy, H.L. Han, L.M. Carl, G.A. Somorjai, Molecular orientations change reaction kinetics and mechanism: A review on catalytic alcohol oxidation in gas phase and liquid phase on size-controlled Pt nanoparticles, Catalysts. 8 (2018) 1–16. https://doi.org/10.3390/catal8060226.

[34] S. Wasmus, W. Vielstich, Methanol oxidation at carbon supported Pt and Pt-Ru electrodes: an on line MS study using technical electrodes, J. Appl. Electrochem. 23 (1993) 120–124. https://doi.org/10.1007/BF00246948.

[35] H. Wang, Z. Jusys, R.J. Behm, Ethanol electro-oxidation on carbon-supported Pt, PtRu and Pt3Sn catalysts: A quantitative DEMS study, J. Power Sources. 154 (2006) 351–359. https://doi.org/https://doi.org/10.1016/j.jpowsour.2005.10.034.

[36] C.J. Bondue, Z. Liang, M.T.M. Koper, Dissociative Adsorption of Acetone on Platinum Single-Crystal Electrodes, J. Phys. Chem. C. 4 (2021). https://doi.org/10.1021/acs.jpcc.0c11360.